

Accepted Article

Title: On the Interaction Between Deprotonated Cytosine (C-H) and Ba²⁺: Infrared Multiphoton spectroscopy and dynamics

Authors: Andrés Felipe Cruz-Ortiz, Martín Ignacio Taccone, Philippe Maitre, Maximiliano Rossa, and Gustavo Ariel Pino

This manuscript has been accepted after peer review and appears as an Accepted Article online prior to editing, proofing, and formal publication of the final Version of Record (VoR). This work is currently citable by using the Digital Object Identifier (DOI) given below. The VoR will be published online in Early View as soon as possible and may be different to this Accepted Article as a result of editing. Readers should obtain the VoR from the journal website shown below when it is published to ensure accuracy of information. The authors are responsible for the content of this Accepted Article.

To be cited as: *ChemPhysChem* 10.1002/cphc.202000696

Link to VoR: <https://doi.org/10.1002/cphc.202000696>

“On the Interaction Between Deprotonated Cytosine (C-H) and Ba²⁺: Infrared Multiphoton spectroscopy and dynamics”

Dr. Andrés F. Cruz-Ortiz,^{a,b,c} Dr. Martín I. Taccone,^{a,b,c} Dr. Philippe Maitre,^d Dr. Maximiliano Rossa^{a,b,c} and Prof. Gustavo A. Pino^{a,b,c,*}

^a INFIQC (CONICET-UNC), Ciudad Universitaria, Pabellón Argentina, 5000 Córdoba, Argentina.

^b Departamento de Físicoquímica, Fac. de Ciencias Químicas, Universidad Nacional de Córdoba, Ciudad Universitaria, Pabellón Argentina, X5000HUA Córdoba, Argentina.

^c Centro Láser de Ciencias Moleculares, Universidad Nacional de Córdoba, Ciudad Universitaria, Pabellón Argentina, X5000HUA Córdoba, Argentina.

^d Université Paris-Saclay, CNRS, Institut de Chimie Physique, 91405, Orsay, France.

*Corresponding author: gpino@unc.edu.ar

Accepted Manuscript

ABSTRACT

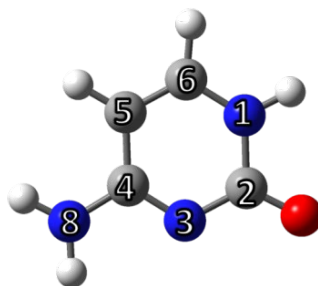
Gas-phase interactions between Ba^{2+} and deprotonated cytosine ($\text{C}_{(-\text{H})}$) were studied in $[\text{C}_{(-\text{H})}\text{Ba}]^+$ and $[\text{C}_{(-\text{H})}\text{BaC}]^+$ complexes by IRMPD spectroscopy coupled to tandem mass-spectrometry in combination with DFT calculations. For the $[\text{C}_{(-\text{H})}\text{BaC}]^+$ complex only one $[\text{C}_{(-\text{H})}\text{KAN10-Ba-C}_{\text{anti}}]^+$ isomer was found, although the presence of another structure cannot be neglected. This isomer features a central tetracoordinated Ba^{2+} that simultaneously interacts with keto-amino $[\text{C}_{(-\text{H})}]^-$ deprotonated on N1 and neutral keto-amino C. Both moieties are in different planes as a consequence of an additional $\text{NH}\cdots\text{O}=\text{C}$ hydrogen bond between C and $[\text{C}_{(-\text{H})}]^-$. A sequential IRMPD dynamics is observed in this complex. For the $[\text{C}_{(-\text{H})}\text{Ba}]^+$ complex produced by electrospray ionization two isomers ($[\text{C}_{(-\text{H})}\text{KAN10Ba}]^+$ and $[\text{C}_{(-\text{H})}\text{KAN30Ba}]^+$) were identified, in which Ba^{2+} interacts simultaneously with the C=O group and the N1 or N3 atom of the keto-amino $[\text{C}_{(-\text{H})}]^-$, respectively. A comparison with the related $[\text{C}_{(-\text{H})}\text{Pb}]^+$ complex (J-Y. Salpin et al., *Chem. Phys. Chem.* **2014**, 15, 2959–2971) is also presented.

INTRODUCTION

Metal cations play a fundamental role in many biological processes through their binding to biomolecules which greatly influences their structure and reactivity. In particular, the double helix structure of DNA^[1] is stabilized by the interaction of the phosphate groups with metal cations, thus partially neutralizing the negative charge.^[2] Interestingly, it has been found that metal cations can also interact specifically with DNA bases. These interactions are structurally important because the metal binds cytosine, guanine, adenine, and thymine (C, G, A, T, respectively) on some of the atoms responsible for the Watson-Crick (WC) hydrogen-bond (H-bond) patterns.^[3] As a result, non-canonical base pairs are formed, thereby stabilizing higher order structures of DNA, i.e., the so-called non-canonical folding. Among the best known non-canonical folds the G-quadruplex is known to be stabilized by metal mono- and/or di-valent cations.^[4-6] Others such as *i-motif*^[7-10] and Hoogsteen^[11,12] non-canonical types are generally proton stabilized and thus found at acid pH. However, they can also be strongly stabilized by Ag⁺^[13-16] or other metal cations (Na⁺, Li⁺, K⁺, Cu⁺)^[17] at neutral pH.

Due to the abundance of both endo- and exogenous metal cations in biological systems, it is important to unravel the nature of their interactions with DNA bases. In this sense, the detailed study at the molecular level, in gas phase, free of the environmental and solvent effects, allows knowing the intrinsic properties that induce the stabilization of non-canonical base pairs and non-canonical tautomers of DNA bases upon interaction with metal cations.

During the last decade the coupling of action UV and/or IR spectroscopies to tandem mass spectrometers (MS/MS) equipped with Electrospray Ionization (ESI) sources has allowed forming, trapping and manipulating ionic complexes of DNA bases with H⁺ or metal cations, and spectroscopically characterizing them.^[6,9,10,12,16-23] Particularly, Infrared Multiphoton Dissociation (IRMPD) spectroscopy using tunable Free Electron Lasers (FEL) is a powerful tool to assign the structure of biomolecular ions. IRMPD spectroscopy coupled to MS/MS has been extensively used to study the interactions between the canonical form of neutral C and H⁺,^[18-21] as well as alkaline, alkaline earth and transition metal cations.^[16,17,22,23] Despite the abundance of divalent cations in biological systems, there are no many IRMPD studies on their interaction with DNA bases.^[24] However, more information is available about the interaction of these M²⁺ with deprotonated.



Scheme 1. Atom numbering of the CKA-N1 tautomer of neutral canonical cytosine.

Among the pyrimidine bases, the interactions of deprotonated uracil ($U_{(-H)}$) with divalent cations have been the most widely studied, using in particular IRMPD spectroscopy integrated to MS/MS. The structures of the $[U_{(-H)}M]^+$ (where $U_{(-H)}$ stands for the deprotonated uracil anion and $M = Pb^{2+}, Cu^{2+}$),^[25-27] $[U_{(-H)}M(H_2O)_n]^+$, and $[U_{(-H)}MU]^+$ (with $M = Pb^{2+}, Cu^{2+}, Zn^{2+}, Mg^{2+}, Ca^{2+}, Sr^{2+}, Ba^{2+}$)^[28-31] complexes have been characterized, whereas in the case of T and C only their interactions with Pb^{2+} ^[25, 32] have been reported. A selective stabilization of one tautomer of $[U_{(-H)}]^-$ was observed depending on the nature of the metal cation. More precisely, it has been found that $[U_{(-H)}]^-$ deprotonated on N3 is stabilized upon interaction with alkaline earth metal cations^[28-30] or Pb^{2+} ,^[25,27] while $[U_{(-H)}]^-$ deprotonated on N1 is stabilized when interacting with Cu^{2+} .^[26]

Much less is known on the interactions between C and divalent cations. There is currently only one experimental work by Salpin *et al.*^[32], reporting that the interaction with Pb^{2+} stabilizes $[C_{(-H)}]^-$, as deprotonated in N1 or N8 of the NH_2 group (see scheme 1). Consequently, the interaction of the resulting anion with the metal cation leading to $[C_{(-H)}Pb]^+$ complexes takes place mostly on N1–Pb–O and N8–Pb–N3, respectively.

In this context, in the present work we present an experimental and theoretical study by means of MS/MS coupled to IRMPD spectroscopy performed with the FEL at the Centre Laser Infrarouge d'Orsay (CLIO) in combination with DFT electronic structure calculations to obtain relevant information regarding the interaction between Ba^{2+} and one or two C molecules and on the dynamics of the IRMPA process.

METHODOLOGY

Experimental Details:

All reagents (from Sigma-Aldrich) were used without further purification. A solution of Cytosine and $BaCO_3$ in equal concentrations (1.0 mM) was prepared using a mixture of MeOH/ H_2O milliQ 1:1 as solvent. This solution was vaporized and ionized using an Electrospray Ionization (ESI) source, coupled to a 7T Fourier-transform ion cyclotron resonance mass spectrometer (7T FT-ICR, Bruker Apex Qe).^[33] Both $[C_{(-H)}Ba]^+$ and $[C_{(-H)}BaC]^+$ ions at m/z 247.94 and 358.97, respectively, were observed. $[C_{(-H)}Ba]^+$ or $[C_{(-H)}BaC]^+$ ions were mass-selected using the quadrupole interface. They were then transferred to, and accumulated in a hexapolar ion trap, where they were thermalised through multiple low-energy collisions with the buffer gas (Ar) before being extracted towards the ICR cell to be further fragmented by IRMPD in the range of 1150–1800 cm^{-1} using the FEL of CLIO,^[34] with the assistance of a CO_2 laser.^[35] The $[C_{(-H)}Ba]^+$ and $[C_{(-H)}BaC]^+$ ions were irradiated during 200 ms with IR-FEL radiation. In the case of the $[C_{(-H)}Ba]^+$ complex, each FEL pulse was followed by a 5 ms CO_2 laser pulse to enhance the fragmentation efficiency.

IRMPD spectra were obtained as the fragmentation efficiency (*Eff*) calculated according to Eq. 1, as a function of the laser frequency.

$$IRMPD \text{ yield} = -\text{Ln} \left(\frac{I_p}{[I_p + \sum I_{frag}]} \right) \quad (1)$$

where, I_p is the intensity of the precursor ion signal and I_{frag} corresponds to the intensity of the fragment ions signals resulting from photofragmentation. In addition, mass-resolved IRMPD spectra are also presented where only one fragment ion is considered.

Computational Details:

All calculations for the different isomers of $[C_{(-H)}Ba]^+$ and $[C_{(-H)}BaC]^+$ complexes were performed at the Density Functional Theory (DFT) level with Gaussian 09 Revision E.01.^[36] The geometries were optimized using the hybrid correlation and exchange B3LYP functional^[37,38] and the 6-311G++(d,p) basis set for the C, H, O and N atoms, while for Ba the effective-core pseudo-potential ECP46MDF developed by Lim et al.^[39] was used. All geometry optimizations were performed on counterpoise corrected potential energy surfaces (PES).^[40] Some additional calculations were also performed using the M06-2X functional and the 6-311G++(d,p) basis set.

The calculations of the IR linear absorption spectra for each of the local minima on the PES were performed at the same theory level. The vibrational frequencies were scaled by 0.9689, as considered the most appropriate scaling factor value for the theory level employed.^[41] For a better comparison with the IRMPD spectra, each calculated IR band was convolved by a Gaussian profile assuming a bandwidth of 15 cm^{-1} at the full width half maximum (FWHM) for complex $[C_{(-H)}Ba]^+$. Indeed, it has been shown that the IRMPD bandwidth is essentially controlled by the IR-FEL bandwidth which is typically on the order of 15 cm^{-1} in the spectral region studied ($1150\text{--}1800 \text{ cm}^{-1}$). In order to get more information on the nature of the Ba-base interactions in the $[C_{(-H)}Ba]^+$ and $[C_{(-H)}BaC]^+$ complexes, Natural Bond Orbitals (NBO) analysis was carried out with the NBO 3.1 program^[42] implemented in Gaussian 09.

The relative Gibbs energies at 298K for the different isomers of $[C_{(-H)}Ba]^+$ and $[C_{(-H)}BaC]^+$ complexes, including the zero point energy corrections (ZPE) were calculated at the same theory level. This temperature compares to that established for multiple collisions with Ar in the hexapolar ion trap of the hybrid mass spectrometer 7T FT-ICR.^[33,43] Finally, the effect of the solvent on the stability of the different isomers of the $[C_{(-H)}Ba]^+$ and $[C_{(-H)}BaC]^+$ complexes was evaluated by the self-consistent reaction field method (SCRF). In this work we used the polarizable continuum model (PCM)^[44] and water as solvent.

RESULTS

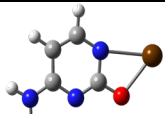

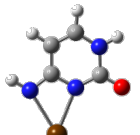

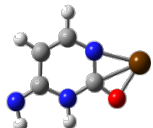
IRMPD Spectroscopy of the $[C_{(-H)}Ba]^+$ complex:

Fragmentation of the $[C_{(-H)}Ba]^+$ complex leads mainly to a loss of H_2O producing the $[C_{(-H)}Ba - H_2O]^+$ fragment (m/z 229.9). $HCNO$ loss leading to a $[C_{(-H)}Ba - HNC O]^+$

fragment (m/z 204.9) is a negligible fragmentation channel. This is in contrast to the fragmentation ratio observed upon IRMPD of complexes of cytosine and other mono- and di-valent cations (Ag^+ , Pb^{2+}).^[23,32] The spectra recorded on the masses of these two fragments show the same spectral features, as observed in Figure S1b, suggesting that they are competing fragmentation channels from the same isomer(s).

Table 1 shows the relative energies of the most stable isomers of the $[\text{C}_{(-\text{H})}\text{Ba}]^+$ complex within 16 kcal/mol in the gas phase, and the corresponding energies corrected for solvent effects. These structures were computed considering the most abundant isomers of $[\text{C}_{(-\text{H})}]^-$ anion, as shown in Table S1.

Table 1. Relative energies including zero point energy corrections (EE+ZPE) and relative standard Gibbs energies calculated at 298K (ΔG°) for the isomers of $[\text{C}_{(-\text{H})}\text{Ba}]^+$ complex and their corresponding dipolar moments (μ) in the gas phase, and the correction of relative energies considering the effect of the solvent (PCM). Relative populations (R.P.) were calculated assuming a Boltzmann distribution, considering that the temperature of the ions is approximately 298 K.

Structure	Gas phase				PCM (water)		
	EE+ZPE (kcal/mol)	$\Delta G^\circ_{298\text{K}}$ (kcal/mol)	R.P.	μ_{gas} (D)	EE+ZPE (kcal/mol)	$\Delta G^\circ_{298\text{K}}$ (kcal/mol)	R.P.
 $[\text{C}_{(-\text{H})}\text{KAN10-Ba}]^+$	0	0	1	7.8	0	0	1
 $[\text{C}_{(-\text{H})}\text{KAN3O-Ba}]^+$	7.4	7.2	6×10^{-6}	10.6	0.6	0.3	0.65
 $[\text{C}_{(-\text{H})}\text{KI}^{\text{N1}}_{\text{anti}},\text{N3N8-Ba}]^+$	5.4	5.4	1×10^{-4}	6.6	7.3	7.0	7×10^{-6}
 $[\text{C}_{(-\text{H})}\text{KI}^{\text{N3}}_{\text{anti}},\text{N1O-Ba}]^+$	13.0	13.0	3×10^{-10}	11.9	5.6	5.4	1×10^{-4}
 $[\text{C}_{(-\text{H})}\text{KI}^{\text{N3}}_{\text{syn}},\text{N1O-Ba}]^+$	15.3	15.9	2×10^{-12}	12.4	8.8	8.9	3×10^{-7}

The IRMPD *Eff* spectrum of the $[C_{(-H)}\text{-Ba}]^+$ complex recorded between 1150 and 1800 cm^{-1} , together with the spectra calculated for the three lowest energy isomers in the gas phase are shown in Figure 1. The IRMPD *Eff* spectrum was determined according to eq. 1 and considering the two fragmentation channels and is shown in Figure 1a. The comparison of the IRMPD spectrum with the spectra calculated for the other isomers is shown in Figure S2. The absence of any band in the 1650-1700 cm^{-1} region corresponding to the free C=O stretching mode of the $[C_{(-H)}\text{KI}_{anti}^{N1}N3N8\text{-Ba}]^+$ isomer and to the C4-N8 stretching mode of the $[C_{(-H)}\text{KI}_{anti}^{N3}N10\text{-Ba}]^+$ and $[C_{(-H)}\text{KI}_{syn}^{N3}N10\text{-Ba}]^+$ isomers (Figure S2) suggests that these structures are not formed under our experimental conditions.

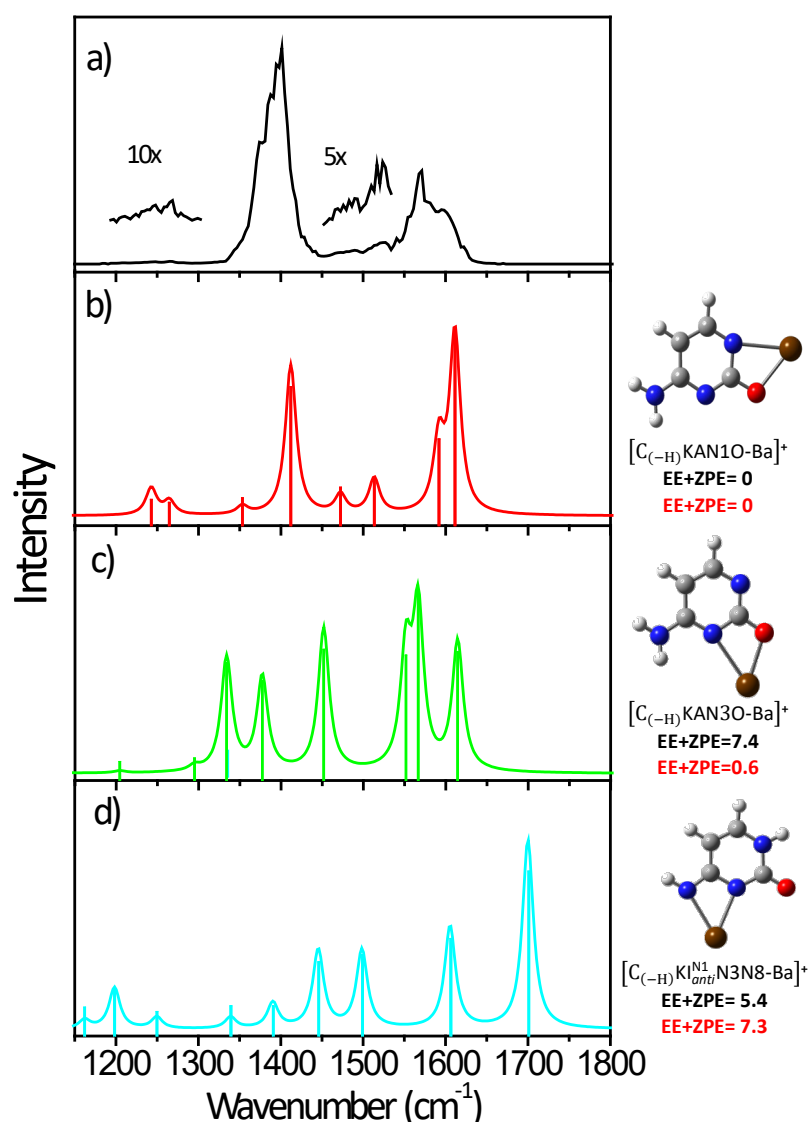


Figure 1. Comparison of the experimental IRMPD *Eff* spectrum of the $[C_{(-H)}\text{Ba}]^+$ complex with the lineal IR spectra calculated at B3LYP/6-311G++ (d,p) and ECP46MDF level for the three lowest energy isomers. a) Experimental, b) $[C_{(-H)}\text{KAN10-Ba}]^+$, c) $[C_{(-H)}\text{KAN30-Ba}]^+$ and d) $[C_{(-H)}\text{KI}_{anti}^{N1}N3N8\text{-Ba}]^+$. The relative energies are reported in kcal/mol with respect to global minimum $[C_{(-H)}\text{KA-N10Ba}]^+$ in the gas (black numbers) and solution (red numbers) phase.

The two remaining structures, $[\text{C}_{(-\text{H})}\text{KAN10-Ba}]^+$ and $[\text{C}_{(-\text{H})}\text{KAN30-Ba}]^+$ correspond to planar structures in which Ba^{2+} interacts simultaneously with the C=O group and either N1 or N3 deprotonated heteroatom of $[\text{C}_{(-\text{H})}]^-$, respectively. Interestingly, the C=O stretching modes of the $[\text{C}_{(-\text{H})}\text{KAN10-Ba}]^+$ and $[\text{C}_{(-\text{H})}\text{KAN30-Ba}]^+$ isomers calculated at 1412 cm^{-1} and 1377 cm^{-1} , respectively, are considerably red shifted with respect to the free C=O band calculated at 1591 cm^{-1} for free $[\text{C}_{(-\text{H})}]^-$. This strong red shifting is due to the increased reduced mass of the C=O stretching mode as a consequence of the strong coupling with the Ba^{2+} cation and the weakening of the C=O bond resulting of this interaction. This is in particular evidenced by the elongation of the C=O bond distance, from 1.238 \AA in the free $[\text{C}_{(-\text{H})}]^-$ to 1.307 \AA and 1.310 \AA in the $[\text{C}_{(-\text{H})}\text{KAN10-Ba}]^+$ and $[\text{C}_{(-\text{H})}\text{KAN30-Ba}]^+$ isomers, respectively.

It is apparent that the shape and width of the band in the $1550\text{--}1630\text{ cm}^{-1}$ spectral region corresponding to the NH_2 bending modes cannot be accounted for assuming that only the most stable $[\text{C}_{(-\text{H})}\text{KAN10-Ba}]^+$ isomer is formed. One hypothesis could be that on the red-side of the broadband near 1570 cm^{-1} is due to the contribution of the $[\text{C}_{(-\text{H})}\text{KAN30-Ba}]^+$ isomer. On the bases of the present results none of the two isomers can be ruled out and this topic will be discussed latter.

IRMPD Spectroscopy of the $[\text{C}_{(-\text{H})}\text{BaC}]^+$ complex:

Two fragments are observed upon IRMPD fragmentation of the $[\text{C}_{(-\text{H})}\text{BaC}]^+$ complex. Loss of a neutral base C leading to a $[\text{C}_{(-\text{H})}\text{Ba}]^+$ fragment is observed as in the case of the related $[\text{U}_{(-\text{H})}\text{BaU}]^+$ complex.^[30] In addition, however, an ionic fragment was detected at a lower intensity, corresponding to the loss of $(\text{C} + \text{H}_2\text{O})$. The two fragmentation channels were considered to obtain the IRMPD *Eff* spectrum (Figure 2a) according to Eq.1. Additionally, mass-resolved IRMPD spectra considering only one of the two ($[\text{C}_{(-\text{H})}\text{Ba}]^+$ or $[\text{C}_{(-\text{H})}\text{Ba} - \text{H}_2\text{O}]^+$) fragments are shown in Figure 2b. As can be seen in this figure, these two mass-resolved IRMPD spectra have different spectral features. The origin of the two fragments and the fragmentation mechanism are two topics of the discussion section.

Table 2 shows the structures and relative stabilities of the five most stable isomers of the $[\text{C}_{(-\text{H})}\text{BaC}]^+$ complex, calculated in both gas and solution phases. In all cases the keto-amino (KA) canonical tautomer of neutral C was considered to interact with Ba^{2+} along with different tautomeric forms of $[\text{C}_{(-\text{H})}]^-$. Noteworthy, no planar structures $[\text{C}_{(-\text{H})}\text{BaC}]^+$ were found below 15 kcal/mol neither in the gas-phase nor in solution, which is in contrast with the findings for $[\text{C-H-C}]^{+[9,10,21]}$ and $[\text{C-M-C}]^+$ (M = alkali metals, Ag^+ , Cu^+) complexes^[16,17] involving two neutral cytosines.

The most stable $[\text{C}_{(-\text{H})}\text{BaC}]^+$ isomers feature a central tetracoordinated Ba^{2+} cation with $[\text{C}_{(-\text{H})}]^-$ and neutral C in two different planes. It is known that tetrahedral structures are usually found when monodentate ligands coordinate the Ba^{2+} cation as in $\text{Ba}^{2+}(\text{H}_2\text{O})_4$.^[45] Forming such a tetrahedral structure for $[\text{C}_{(-\text{H})}\text{BaC}]^+$ would require for the planes of the $[\text{C}_{(-\text{H})}]^-$ and C ligands, which both di-coordinate Ba^{2+} through N and O atoms, to orientate perpendicularly to each other. It seems that the skewed orientation of the

$[C_{(-H)}]^-$ and C subunits around Ba^{2+} in the two lowest-lying isomers, *i.e.*, $[C_{(-H)}KAN10-Ba-C_{anti}]^+$ and $[C_{(-H)}KAN30-Ba-C_{anti}]^+$, is due to an extra intermolecular H-bond between the two ligands (see Table 2). This Ba^{2+} coordination pattern, including a single stabilizing H-bond closely resembles the one found for related complexes of other pyrimidine bases, *i.e.*, the lowest energy $[U_{(-H)}BaU]^+$ isomers.^[29,30]

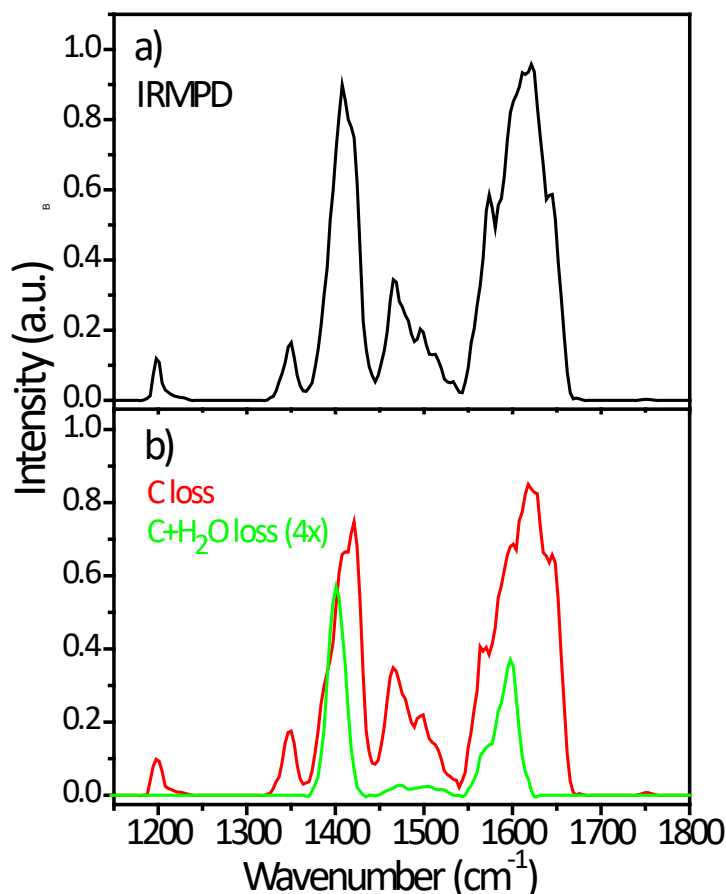
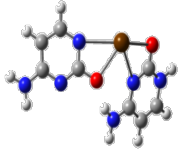
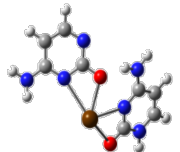
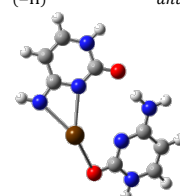
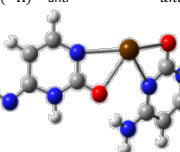
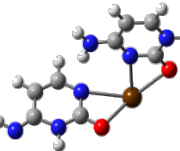


Figure 2. a) IRMPD *Eff* spectrum considering the two fragmentation channels, b) fragments produced from the $[C_{(-H)}BaC]^+$ complex after irradiation with IR photons.

Calculations indicate that the five lowest energy structures are within 15.6 kcal/mol and 7.8 kcal/mol in the gas phase and in solution, respectively. The global minimum in both gas phase and aqueous solution corresponds to the $[C_{(-H)}KAN10-Ba-C_{anti}]^+$. In this isomer, Ba^{2+} interacts simultaneously with N1 and O of $[C_{(-H)}]^-$, which is found in its KA form. Among the different conformations of this isomer, the *anti*-conformation is likely to be favored because of the additional stabilization induced by the formation of the $NH\cdots O=C$ hydrogen bond between the NH_2 group of C and the C=O group of $[C_{(-H)}]^-$. Consequently, and regardless of the initial conformational orientation of both C and $[C_{(-H)}]^-$, all the structures evolved spontaneously during the optimization towards the *anti*-conformation of the neutral C ligand.

Table 2. Relative energies including zero point energy corrections (EE+ZPE) and relative standard Gibbs energies calculated at 298K (ΔG°) for the isomers of the $[C_{(-H)}BaC]^+$ complex and their corresponding dipolar moments (μ) in gas phase and the correction of relative energies considering the effect of the solvent (PCM). Relative populations (R.P.) were calculated assuming a Boltzmann distribution, considering that the temperature of the ions is approximately 298 K.

Structure	Gas phase				PCM (Water)		
	EE+ZPE (kcal/mol)	ΔG°_{298K} (kcal/mol)	R.P.	μ_{gas} (D)	EE+ZPE (kcal/mol)	ΔG°_{298K} (kcal/mol)	R.P.
 $[C_{(-H)}KAN10-Ba-C_{anti}]^+$	0	0	1	4.0	0	0	1
 $[C_{(-H)}KAN30-Ba-C_{anti}]^+$	5.3	2.3	1×10^{-4}	5.7	1.1	0.8	0.25
 $[C_{(-H)}KI_{anti}^{N1}N3N8-Ba-C_{anti}]^+$	10.9	13.0	3×10^{-10}	3.5	7.8	4.9	3×10^{-4}
 $[C_{(-H)}KI_{anti}^{N3}N10-Ba-C_{anti}]^+$	12.9	6.2	3×10^{-5}	9.3	5.5	4.4	5×10^{-4}
 $[C_{(-H)}KI_{anti}^{N3}N10-Ba-C_{syn}]^+$	15.6	15.3	6×10^{-12}	10.0	6.8	10.9	1×10^{-8}

The linear IR absorption spectra of the five lowest-lying structures of $[C_{(-H)}BaC]^+$ were compared with the corresponding IRMPD spectrum (Figure S3). The $[C_{(-H)}KI_{anti}^{N3}N10-Ba-C_{anti}]^+$, $[C_{(-H)}KI_{anti}^{N3}N10-Ba-C_{syn}]^+$ and $[C_{(-H)}KI_{anti}^{N1}N3N8-Ba-C_{anti}]^+$ isomers are significantly higher in energy than the other two isomers, either in the gas or aqueous solution. Therefore, a very low population of these isomers is expected at the experimental temperature (~ 300 K, see Table 2); hence they are dismissed in the following discussion. On the other hand, predicted energy differences of $[C_{(-H)}KAN10-Ba-C_{anti}]^+$ $[C_{(-H)}KAN30-Ba-C_{anti}]^+$ isomers is small in both gas and solution phase, so that one could consider that both structures may be at play under our experimental conditions.

Figure 3 shows the comparison of the IRMPD *Eff* spectrum with the spectra calculated for the two lowest-energy isomers in the gas phase and solution (See Table 2). As observed in Figure 3 and Table 3, the whole IRMPD *Eff* spectrum could be assigned considering IR transitions predicted for the global minimum $[\text{C}_{(-\text{H})}\text{KAN10-Ba-C}_{anti}]^+$ isomer. However, the presence of the isomer $[\text{C}_{(-\text{H})}\text{KAN30-Ba-C}_{anti}]^+$ cannot be ruled out. Most importantly, comparison of its calculated spectrum to the IRMPD *Eff* spectrum, especially in the 1450-1500 cm^{-1} region, suggests that this isomer could also be formed.

A broad band is observed in the 1450-1500 cm^{-1} region, with a maximum at 1466 cm^{-1} which could be assigned to the in-plane ring-deformation mode (N1-C1 + N3-C4) of $[\text{C}_{(-\text{H})}]^-$ in the $[\text{C}_{(-\text{H})}\text{KAN10-Ba-C}_{anti}]^+$ isomer, calculated at 1463 cm^{-1} . However, the relative intensity observed in the IRMPD *Eff* spectrum for this band is not properly reproduced by the calculations, considering only the $[\text{C}_{(-\text{H})}\text{KAN10-Ba-C}_{anti}]^+$ isomer. One hypothesis could be that this IRMPD band is also due to a band of $[\text{C}_{(-\text{H})}\text{KAN30-Ba-C}_{anti}]^+$, calculated at 1444 cm^{-1} and assigned to the in-plane ring-deformation mode (N1-C1 + N3-C4) of $[\text{C}_{(-\text{H})}]^-$ for this isomer.

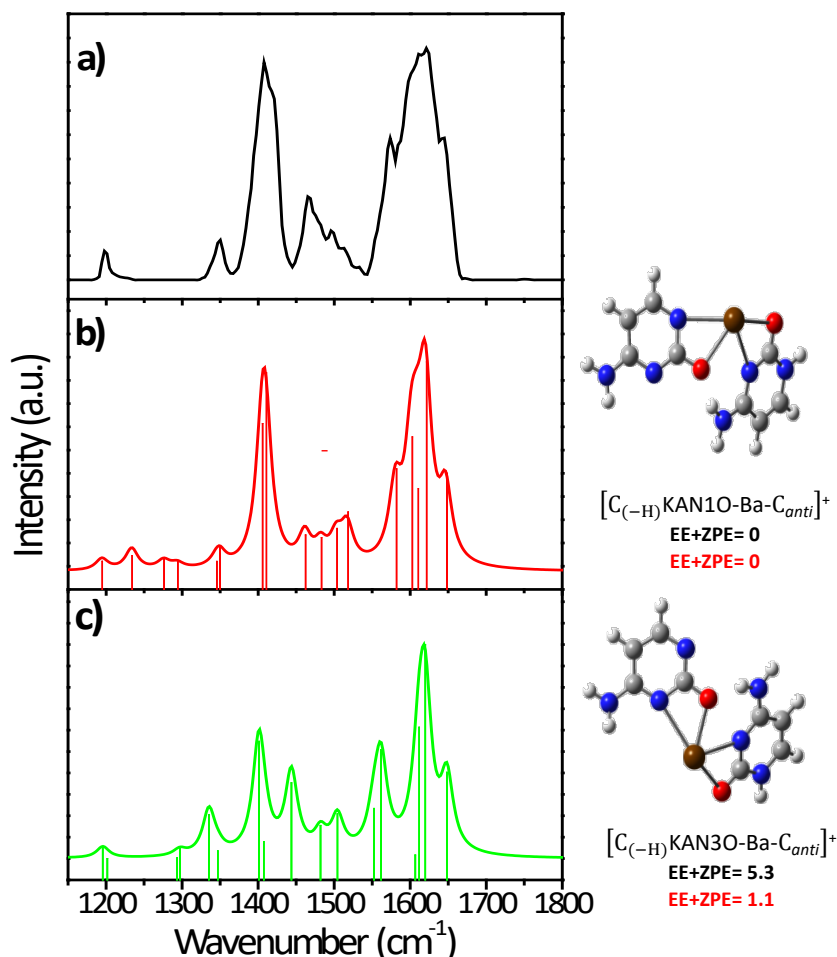


Figure 3. Comparison of the experimental IRMPD *Eff* spectrum of the $[\text{C}_{(-\text{H})}\text{BaC}]^+$ complex with the linear IR spectra calculated at B3LYP/6-311G++(d,p) and ECP46MDF level for the two lowest energy isomers. a) Experimental, b) $[\text{C}_{(-\text{H})}\text{KAN10-Ba-C}_{anti}]^+$, and c) $[\text{C}_{(-\text{H})}\text{KAN30-Ba-C}_{anti}]^+$. The relative energies are reported in kcal/mol with respect to global minimum $[\text{C}_{(-\text{H})}\text{KAN10Ba-C}_{anti}]^+$ in the gas (black numbers) and in solution (red numbers) phase.

The most intense peak observed in the IRMPD spectrum at 1622 cm^{-1} nicely match with predicted bands at 1622 and 1620 cm^{-1} for the $[\text{C}_{(-\text{H})}\text{KAN10-Ba-C}_{anti}]^+$ and $[\text{C}_{(-\text{H})}\text{KAN30-Ba-C}_{anti}]^+$ isomers, respectively. This 1622 cm^{-1} band can thus be assigned to the combination of the C=O and C5–C6 stretching modes of neutral cytosine in both isomers. As expected, the stretching frequency of the C=O bond of CKA-N1, calculated at 1715 cm^{-1} for the free molecule, is shifted to the red as a result of the weakening of this bond due to the direct interaction with Ba^{2+} . This is evidenced by a slight lengthening of the C=O bond distance from 1.216 \AA in free CKA-N1 to 1.249 \AA in the two most stable isomers of the $[\text{C}_{(-\text{H})}\text{BaC}]^+$ complex.

Table 3. Experimental and calculated vibrational frequencies for the two lowest energy isomers of the $[\text{C}_{(-\text{H})}\text{BaC}]^+$ complex, together with their corresponding assignment.

Experimental (cm^{-1})	Calculated (cm^{-1})		Assignment
	$[\text{C}_{(-\text{H})}\text{KAN10-Ba-C}_{anti}]^+$	$[\text{C}_{(-\text{H})}\text{KAN30-Ba-C}_{anti}]^+$	
1198	1195	1195	Balancing C4–N1–H of CKA-N1
1350	1350	1335	$\nu\text{N1-C2}$ and $\nu\text{C5-C8}$ of $[\text{C}_{(-\text{H})}]^+$
1408	1411	1401	$\nu\text{C=O}$ + $\nu\text{N3-C4}$ of $[\text{C}_{(-\text{H})}]^+$
1466	1463	1444	$\nu\text{N1-C2}$ and $\nu\text{N3-C4}$ of $[\text{C}_{(-\text{H})}]^+$
1497	1504	1504	$\nu\text{C4-C5}$ of CKA-N1
1512	1518		$\nu\text{N1-C6}$ + $\nu\text{C4-C5}$ + δNH_2 of $[\text{C}_{(-\text{H})}]^+$
1573	1582		$\nu\text{C5-C6}$ + δNH_2 of $[\text{C}_{(-\text{H})}]^+$
1622	1622	1620	$\nu\text{C=O}$ + C5–C6 of CKA-N1
1645	1649	1648	δNH_2 of CKA-N1

ν = Stretching; δ = Bending

A very weak band is observed at 1750 cm^{-1} in the IRMPD spectrum and in the mass-resolved IRMPD spectrum recorded on the mass of the $[\text{C}_{(-\text{H})}\text{Ba}]^+$ fragment (Figure 2) which is assigned neither to the two most stable isomers nor to the other three isomers presented in Table 2 and Figures S3. Therefore, the contribution of a different isomer cannot be neglected.

DISCUSSION

Kinetic model for the fragmentation mechanism of the $[\text{C}_{(-\text{H})}\text{BaC}]^+$ complex:

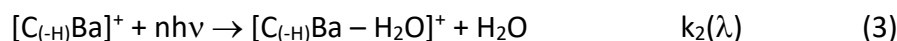
We will first discuss the fragmentation of $[\text{C}_{(-\text{H})}\text{BaC}]^+$, based on the modeling of the mass-resolved IRMPD spectra when $[\text{C}_{(-\text{H})}\text{Ba}]^+$ and $[\text{C}_{(-\text{H})}\text{Ba} - \text{H}_2\text{O}]^+$ are considered separately. The fact that these two spectra have different spectral features could be interpreted in different ways.

The first possibility is that these two fragments may be produced from two different fragmentation channels of the precursor $[\text{C}_{(-\text{H})}\text{BaC}]^+$ ion. Such competitive fragmentation scheme has been reported, for example, for the fragmentation of the *para*-amino benzoil cation.^[46] In such a case, each fragment should be observed at the same wavelengths, and resemble the IRMPD *Eff* spectrum of the precursor ion. As discussed above (see Figure 2), the mass-resolved IRMPD spectra recorded on the mass of the $[\text{C}_{(-\text{H})}\text{Ba-H}_2\text{O}]^+$ or $[\text{C}_{(-\text{H})}\text{Ba}]^+$ fragments are very different one of the other. This could

suggest that the energy randomization is not complete in the time scale of the dissociation. However, this is quite unlikely for systems of this size and at the excitation energy at which the C loss channel is open.

The second possibility is that $[\text{C}_{(-\text{H})}\text{Ba} - \text{H}_2\text{O}]^+$ is a secondary fragment produced by a consecutive IRMP absorption (IRMPA) of the primary $[\text{C}_{(-\text{H})}\text{Ba}]^+$ fragment at wavelengths that are resonant with transitions of both the precursor and fragment ions. Such sequential fragmentation is often observed, and has been discussed in the case of eg. $[\text{Fe}(\text{C}_4\text{H}_8)]^+$,^[47] for which sequential loss of H_2 and butadiene has been observed. In such a case, the mass-resolved IRMPD spectra recorded on the masses of the two observed fragments are expected to be different convolutions of the IRMPD spectrum of the $[\text{C}_{(-\text{H})}\text{BaC}]^+$ precursor ion and the IRMPD spectrum of the $[\text{C}_{(-\text{H})}\text{Ba}]^+$ primary fragment ion.

In order to challenge this hypothesis, the following kinetic model was used to simulate the convoluted spectra of the fragments:



where $k_1(\lambda)$ and $k_2(\lambda)$ are proportional to the calculated wavelength-dependent IR absorption cross-section ($\sigma_1(\lambda)$ and $\sigma_2(\lambda)$) for the $[\text{C}_{(-\text{H})}\text{BaC}]^+$ and $[\text{C}_{(-\text{H})}\text{Ba}]^+$ ions, respectively. Integrating the differential equations for this kinetic model, the intensity of both fragments as a function of the wavelength is obtained as follows:

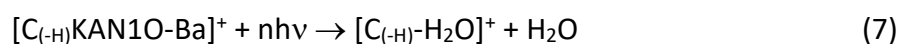
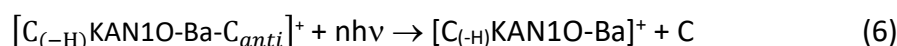
$$I_{[\text{C}_{(-\text{H})}\text{Ba}]^+}(\lambda) = \frac{\sigma_1(\lambda)}{\sigma_2(\lambda) - \sigma_1(\lambda)} [\exp(-\sigma_1(\lambda)\alpha) - \exp(-\sigma_2(\lambda)\alpha)] \quad (4)$$

$$I_{[\text{C}_{(-\text{H})}\text{Ba} - \text{H}_2\text{O}]^+}(\lambda) = 1 - \frac{1}{\sigma_2(\lambda) - \sigma_1(\lambda)} [\sigma_2(\lambda) \exp(-\sigma_1(\lambda)\alpha) - \sigma_1(\lambda) \exp(-\sigma_2(\lambda)\alpha)] \quad (5)$$

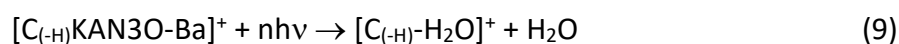
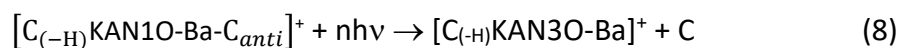
where α is a proportionality constant accounting for the irradiation time and laser fluence (photon density).

Assuming that the $[\text{C}_{(-\text{H})}\text{BaC}]^+$ complex is mainly observed in its $[\text{C}_{(-\text{H})}\text{KAN10-Ba-C}_{anti}]^+$ isomeric form as assigned above, the calculated IR spectrum of this isomer was used to derive $\sigma_1(\lambda)$ for the kinetic simulation and two different likely fragmentations were considered:

Case a: The $[\text{C}_{(-\text{H})}\text{KAN10-Ba-C}_{anti}]^+$ isomer fragments to the $[\text{C}_{(-\text{H})}\text{KAN10-Ba}]^+$ isomer only.

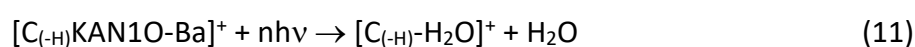
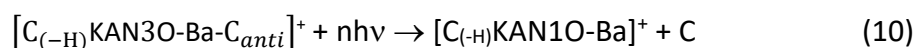


Case b: The $[\text{C}_{(-\text{H})}\text{KAN10-Ba-C}_{anti}]^+$ isomer fragments to the $[\text{C}_{(-\text{H})}\text{KAN30-Ba}]^+$ isomer only.

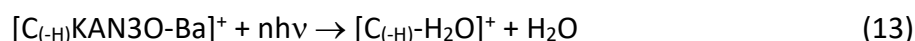
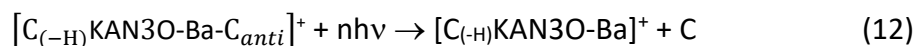


In addition, we also considered the cases in which the $[\text{C}_{(-\text{H})}\text{KAN3O-Ba-C}_{anti}]^+$ isomeric form of the $[\text{C}_{(-\text{H})}\text{BaC}]^+$ complex fragments to $[\text{C}_{(-\text{H})}\text{KAN1O-Ba}]^+$ or $[\text{C}_{(-\text{H})}\text{KAN3O-Ba}]^+$. The calculated IR spectrum of this isomer was used to derive $\sigma_1(\lambda)$ for the kinetic simulation of the two fragmentation cases:

Case c: The $[\text{C}_{(-\text{H})}\text{KAN3O-Ba-C}_{anti}]^+$ isomer fragments to the $[\text{C}_{(-\text{H})}\text{KAN1O-Ba}]^+$ isomer only.



Case d: The $[\text{C}_{(-\text{H})}\text{KAN3O-Ba-C}_{anti}]^+$ isomer fragments to the $[\text{C}_{(-\text{H})}\text{KAN3O-Ba}]^+$ isomer only.



To perform the simulations, two sets of $\sigma_2(\lambda)$ functions were obtained from the corresponding calculated IR spectra of $[\text{C}_{(-\text{H})}\text{KAN1O-Ba}]^+$ for *cases a* and *c* and $[\text{C}_{(-\text{H})}\text{KAN3O-Ba}]^+$ for *case b* and *d*, respectively.

The simulated mass-resolved spectra, along with the simulated IRMPD *Eff* spectrum for all cases are shown in Figure 4 where they are compared with the corresponding experimental spectra. A good agreement between the three experimental and simulated spectra is only observed for *case a*. The agreement with the simulation of the other cases (*b*, *c* and *d*) is not as good since they do not satisfactorily simulate the complete set of three experimental spectra (IRMPD *Eff* and two mass-resolved spectra). These results suggest that the sequential IRMPA mechanism is indeed at play and that the fragmentation of the $[\text{C}_{(-\text{H})}\text{KAN1O-Ba-C}_{anti}]^+$ isomer leads more likely to the $[\text{C}_{(-\text{H})}\text{KAN1O-Ba}]^+$ isomeric fragment than to the $[\text{C}_{(-\text{H})}\text{KAN3O-Ba}]^+$ isomer. This is an expected results since fragmentation to the $[\text{C}_{(-\text{H})}\text{KAN1O-Ba}]^+$ is a direct process, while producing the $[\text{C}_{(-\text{H})}\text{KAN3O-Ba}]^+$ isomer requires the migration of the Ba^{2+} moiety from N1 to N3 with an isomerization energy barrier of 19 kcal/mol. However, a minor contribution from the other fragmentation cases cannot be ruled out in view of the current results.

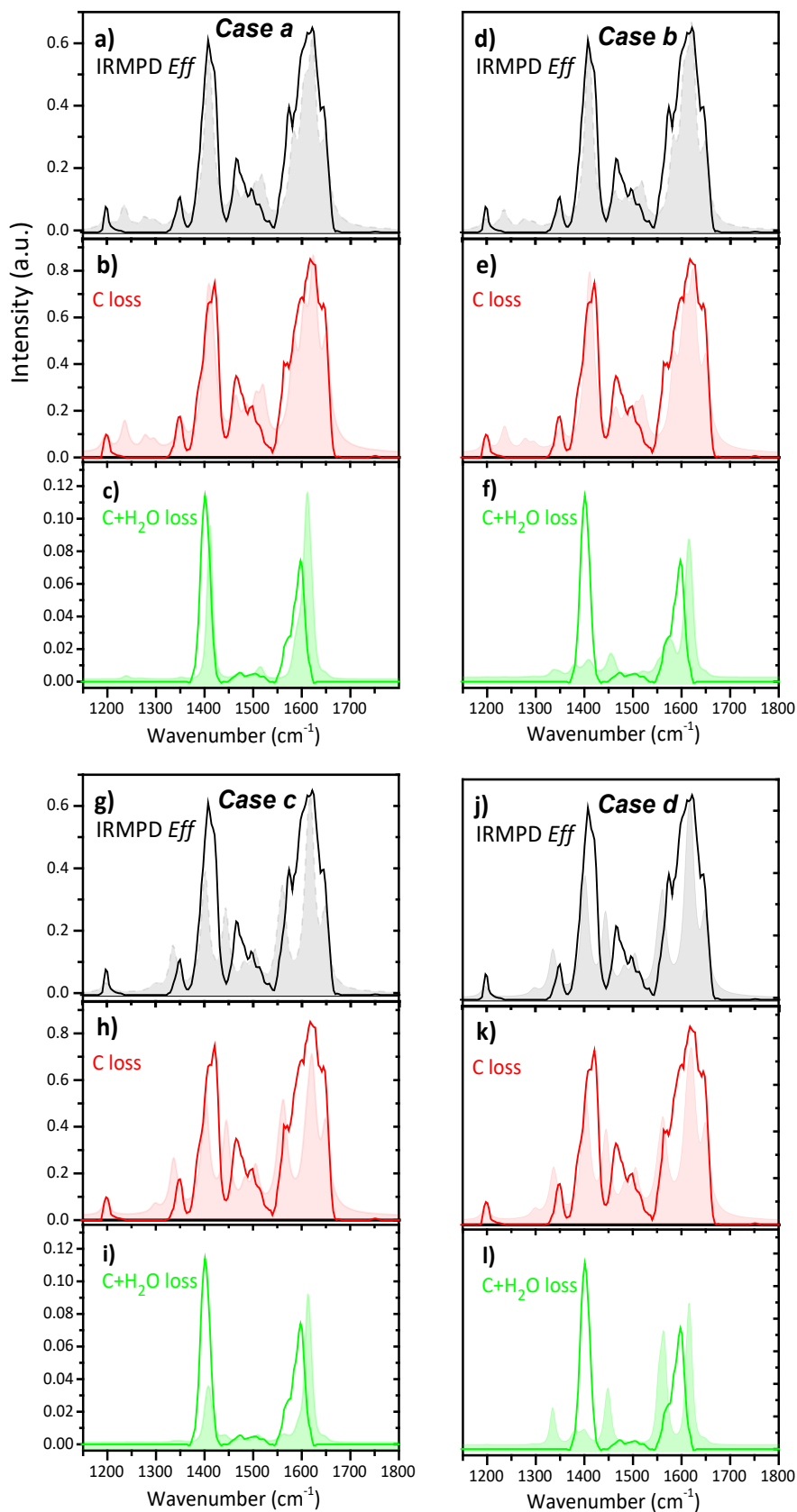


Figure 4. a,d,g,j) IRMPD Eff spectrum of $[C_{(-H)BaC}]^+$ complex and fragments b,e,h,k) Cytosine loss and c,f,i,l) (Cytosine+H₂O) loss obtained after irradiation with IR photons. Experimental (in lines) and simulated from the kinetic models (shaded surface) considering case a (left-upper), case b (right-upper), case c (left-lower), case d (right-lower).

The small bands predicted between 1220 and 1320 cm^{-1} , are not observed neither when the two fragments nor when only the $[\text{C}_{(-\text{H})}\text{Ba}]^+$ fragment (panel a and b, respectively) are considered. Also, the relative intensity of the band at 1600 cm^{-1} in the experimental spectrum recorded on the mass of the $[\text{C}_{(-\text{H})}\text{Ba} - \text{H}_2\text{O}]$ fragment is lower than predicted. The origin of these differences is still uncertain. However, different relative intensities between computed linear IR and experimental IRMPD spectra are often observed, and may arise from the complexity of the multiple-photon nature of the IRMPA process.^[47,48,49]

Isomers assignment of IRMPD vs ESI source generated $[\text{C}_{(-\text{H})}\text{Ba}]^+$ complex:

From the previous discussion, it can be concluded that IRMPA of the $[\text{C}_{(-\text{H})}\text{BaC}]^+$ complex leads to the formation of $[\text{C}_{(-\text{H})}\text{Ba}]^+$ fragment corresponding to the $[\text{C}_{(-\text{H})}\text{KAN10-Ba}]^+$ isomer. The question is whether only this isomer of $[\text{C}_{(-\text{H})}\text{Ba}]^+$ is formed upon ESI.

In Figure 5a, the IRMPD spectrum of $[\text{C}_{(-\text{H})}\text{Ba}]^+$ formed upon ESI is given (black line) as well of the mass-resolved IRMPD spectrum of $[\text{C}_{(-\text{H})}\text{Ba}]^+$ formed upon IRMPA of $[\text{C}_{(-\text{H})}\text{BaC}]^+$ (green line). Although the same dominant spectral features are observed in both spectra, there are some differences that deserve a further analysis.

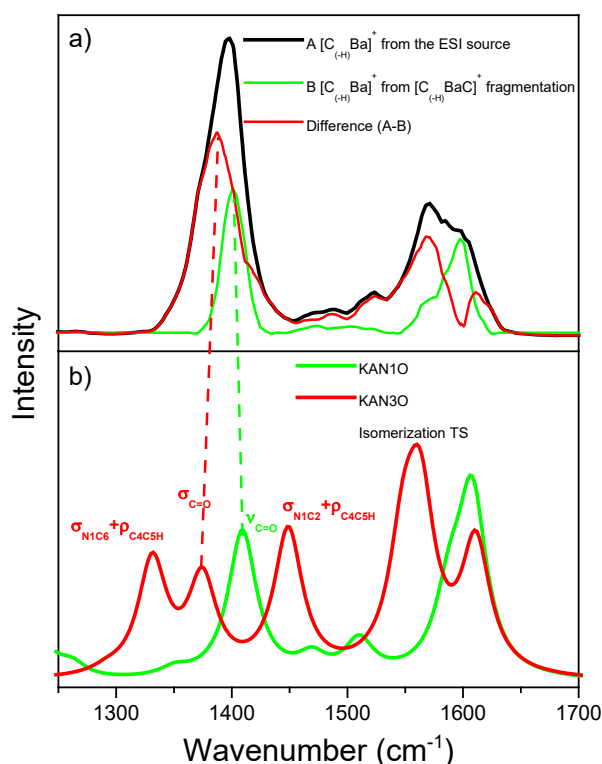


Figure 5. a) IRMPD spectrum of the $[\text{C}_{(-\text{H})}\text{Ba}]^+$ complex produced in the ESI source (black line), as the primary fragment from the IRMPD of $[\text{C}_{(-\text{H})}\text{BaC}]^+$ complex (green line) and the difference between these two spectra (red line). b) Linear IR spectra calculated at B3LYP/6-311G++(d,p) ECP46MDF for the two lowest energy isomers.

To this aim the difference spectrum, which results from subtracting the IRMPD spectrum of $[C_{(-H)}Ba]^+$ generated from IRMPD of the $[C_{(-H)}BaC]^+$ complex (green line), from the IRMPD *Eff* spectrum of $[C_{(-H)}Ba]^+$ produced in the ESI source (black line), is also shown in Figure 5a (red line). The resulting distinct spectral features are suggestive of the presence of at least a second isomer of the $[C_{(-H)}Ba]^+$ complex, which is formed in the ESI source but not produced from the IRMPD of the $[C_{(-H)}BaC]^+$ complex.

The simulated spectra of the $[C_{(-H)}KAN10-Ba]^+$ and $[C_{(-H)}KAN30-Ba]^+$ isomers are shown in Figure 5b. As observed in Figure 5, the mass-resolved IRMPD spectrum of $[C_{(-H)}Ba]^+$ formed upon IRMPA of $[C_{(-H)}BaC]^+$ (panel a; green line) closely resembles the calculated spectrum of the $[C_{(-H)}KAN10-Ba]^+$ isomer in the whole spectral range, while the difference spectrum (Fig. 5a; red line) is in good agreement with the calculated IR spectrum for the $[C_{(-H)}KAN30-Ba]^+$ isomer in the 1525 – 1650 cm^{-1} spectral range, which may be considered as a diagnostic spectral region to assert that both isomers are produced upon ESI. The assignments of the most important bands are shown in Table 4.

Table 4. Selected experimental IR vibrational frequencies for the $[C_{(-H)}Ba]^+$ (in cm^{-1}) and assignment to calculated IR spectra for $[C_{(-H)}KAN10-Ba]^+$ and $[C_{(-H)}KAN30-Ba]^+$ isomers.

Experimental From IRMPD of $[C_{(-H)}BaC]^+$ (green line in Figure 5b) (cm^{-1})	Calculated $[C_{(-H)}KAN10-Ba]^+$ (cm^{-1})	Assignment	Experimental difference spectrum (red line in Figure 5a) (cm^{-1})	Calculated $[C_{(-H)}KAN30-Ba]^+$ (cm^{-1})	Assignment
				1334	$\sigma N1-C6 +$ $\rho C4-C5-H$
Intense 1401	1412	$\sigma C=O$	Intense 1387	1377	$\sigma C=O$
1474	1472	$\sigma N3-C2 +$ $\rho C4-C5-H$		1450	$\sigma N1-C2 +$ $\rho C4-C5-H$
1510	1513	$\sigma N1-C6 +$ $\sigma C4-C5$			
			1525	1551	$\sigma N3-C4 +$ $\sigma C5-C6$
1572	1591	$\beta NH_2 +$ $\sigma C5-C6$	1570	1566	$\beta NH_2 + \sigma C4-C5 +$ $\sigma C2-N1$
1598	1612	βNH_2	1610	1614	βNH_2

σ = Stretching; β = Bending and ρ =Rocking

The discussion of the spectral region 1325-1450 cm^{-1} is not straightforward. In the case of the spectrum of the $[C_{(-H)}Ba]^+$ complex produced from the IRMPD of $[C_{(-H)}BaC]^+$ (Fig. 5a; green line), the experimental intense band at 1401 cm^{-1} is in good agreement with the band calculated at 1412 cm^{-1} , assigned to the C=O stretching mode of the computed spectra for the $[C_{(-H)}KAN10-Ba]^+$ isomer. The red shifting of the experimental band, as compared to the calculated linear IR spectrum can be accounted for on the basis of the increasing internal energy during the IRMPA processes.^[46] However, in the

case of the difference spectrum (Fig. 5a; red line), a number of discrepancies with the computed spectra of the $[C_{(-H)}KAN3O-Ba]^+$ isomer are apparent in this spectral region.

The tentative assignment shown in Table 4 for the most important bands in the 1325-1450 cm^{-1} spectral region indicates an enhanced intensity and an apparent blue-shift of the experimental band at 1387 cm^{-1} , as compared to the theoretical band at 1377 cm^{-1} attributable to the C=O stretching mode in the linear IR spectrum of the $[C_{(-H)}KAN3O-Ba]^+$ isomer. However, the other two bands calculated at 1334 and 1450 cm^{-1} are not clearly observed in the experimental spectrum.

The reasons for the strong disagreement in this spectral region are still unclear. They are probably related to anharmonic effects and/or dynamics effects associated with isomerization upon IRMPA. For instance, it is interesting to note that the IR absorption spectrum predicted for the N1-N3 TS nicely matches the difference IRMPD spectrum (in red, Fig. 5a), as shown in Figure S4 in the supplementary information.

Gas vs. solution phase isomers population:

The assignment of the IRMPD spectrum of the $[C_{(-H)}Ba]^+$ complex allowed identifying the presence of the $[C_{(-H)}KAN1O-Ba]^+$ and $[C_{(-H)}KAN3O-Ba]^+$ isomers when the complex is produced in the ESI source, which are the two most stable structures in aqueous solution, while only the $[C_{(-H)}KAN1O-Ba]^+$ isomer is produced upon IRMPD of the $[C_{(-H)}BaC]^+$ complex.


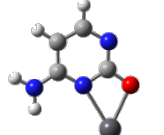

The $[C_{(-H)}KAN3O-Ba]^+$ isomer is the third most stable isomer in the gas phase, but it is energetically slightly above the global minimum in solution (Table 1). The relative populations (R.P.) expected for the $[C_{(-H)}KAN1O-Ba]^+$, $[C_{(-H)}KAN3O-Ba]^+$ and $[C_{(-H)}KI_{anti}^{N1}N3N8-Ba]^+$ isomers in the gas phase are 1.0, 6×10^{-6} , and 1×10^{-4} , respectively, while the corresponding R.P. in the solution are 1.0, 0.65 and 7×10^{-4} . Since experimentally, only the $[C_{(-H)}KAN1O-Ba]^+$ and $[C_{(-H)}KAN3O-Ba]^+$ isomers are observed, it allows suggesting that the isomers population observed in the gas phase most likely resembles the isomers population in the solution, indicating that these structures are maintained upon vaporization of the solution in the soft ESI source, as previously observed in other works for $[CGH]^+$ ^[12] and $[Thd-Na]^+$ ^[50].

The solvent reduces the overall energy difference between the most and the less stable isomers substantially changing their relative stability. The most stabilized isomers by the solvent are those with the highest dipole moment (Table 1). Due to solvent stabilization, the $[C_{(-H)}KAN3O-Ba]^+$ isomer becomes the second most stable structure in solution, almost isoenergetic with the $[C_{(-H)}KAN1O-Ba]^+$ isomer, while the second most stable isomer in the gas phase is $[C_{(-H)}KI_{anti}^{N1}N3N8-Ba]^+$ becomes the fourth energy isomer in solution found at 7.3 kcal/mol above the global minimum.

At variance with the $[C_{(-H)}Ba]^+$ complex, Salpin *et al.*^[32] reported for the $[C_{(-H)}Pb]^+$ complex to be present in the $[C_{(-H)}KAN1O-Ba]^+$ and $[C_{(-H)}KI_{anti}^{N1}N3N8-Ba]^+$ isomeric forms. In order to rationalize this difference, the relative energies of the three most stable isomers of

the $[C_{(-H)}Pb]^+$ complex in the gas phase and in solution were calculated with the theoretical method used in this work, and the results are shown in Table 5.

Table 5. Relative energies including zero point energy corrections (EE+ZPE) and relative standard Gibbs energies calculated at 298K (ΔG°) for the isomers of the $[C_{(-H)}Pb]^+$ complex and their corresponding dipolar moments (μ) in the gas phase, the correction of relative energies considering the effect of the solvent (PCM) Relative populations (R.P.) were calculated assuming a Boltzmann distribution, considering that the temperature of the ions is approximately 298 K.

Structure	Gas phase				PCM (water)		
	EE+ZPE (kcal/mol)	ΔG°_{298K} (kcal/mol)	R.P.	μ_{gas} (D)	EE+ZPE (kcal/mol)	ΔG°_{298K} (kcal/mol)	R.P.
 $[C_{(-H)}KAN10 - Pb]^+$	0	0	1	4.3	0	0	1
 $[C_{(-H)}KAN30 - Pb]^+$	8.23	8.02	1×10^{-6}	6.8	2.41	2.28	0.02
 $[C_{(-H)}KI_{anti}^{N1}N3N8 - Pb]^+$	0.32	0.24	0.66	4.3	1.82	1.75	0.05

From Table 5, it is apparent that in the gas phase the relative stability of the different isomers of the $[C_{(-H)}Pb]^+$ complex is the same as for $[C_{(-H)}Ba]^+$, being the $[C_{(-H)}KI_{anti}^{N1}N3N8-M]^+$ isomer more stable than the $[C_{(-H)}KAN30-M]^+$ isomer ($M = Ba^{2+}$ or Pb^{2+}). However, the solvation effect for $[C_{(-H)}Pb]^+$ is not enough to stabilize the $[C_{(-H)}KAN30-Pb]^+$ isomer below the $[C_{(-H)}KI_{anti}^{N1}N3N8-Pb]^+$ isomer, as it occurs for $[C_{(-H)}Ba]^+$. Thus, in the case of $[C_{(-H)}Pb]^+$ the relative stabilities in the gas phase and in solution are the same.

Therefore, the differences observed between the $[C_{(-H)}Ba]^+$ and $[C_{(-H)}Pb]^+$ complexes are reconciled considering that in both cases, the most stable structures in solution are maintained upon vaporization in the ESI source and observed in the gas phase by IRMPD.

In the $[C_{(-H)}Ba]^+$ complex, the μ of the $[C_{(-H)}KAN30-Ba]^+$ isomer (10.6 D) is 4.0 D larger than that for $[C_{(-H)}KI_{anti}^{N1}N3N8-M]^+$ (6.6 D) (Table 1), while this difference is only 2.5 D for the corresponding isomers of the $[C_{(-H)}Pb]^+$ complex (Table 5). The smaller difference in the dipolar moments could be the reason for the lower relative stabilization

of the $[C_{(-H)}KAN3O-Pb]^+$ isomer upon solvation, than that of the $[C_{(-H)}KAN3O-Ba]^+$ isomer.

CONCLUSIONS

In this work we applied a combined IRMPD spectroscopy and quantum chemical approach to characterize the mass-selected $[C_{(-H)}Ba]^+$ and $[C_{(-H)}BaC]^+$ complexes in the gas phase.

From the analysis of the results it was concluded that the $[C_{(-H)}BaC]^+$ complex is mainly found in its $[C_{(-H)}KAN1O-Ba-C_{anti}]^+$ isomeric form. The IRMPD of this complex leads to the observation of two ionic fragments: $[C_{(-H)}Ba]^+$ and $[C_{(-H)}Ba-H_2O]^+$. The analysis and simulation of the mass-resolved IRMPD spectra on both fragments suggest that $[C_{(-H)}Ba]^+$ in its $[C_{(-H)}KAN1O-Ba]^+$ isomeric form is the primary ionic fragment of the $[C_{(-H)}BaC]^+$ complex, while $[C_{(-H)}Ba-H_2O]^+$ is a secondary fragment produced by the subsequent IRMPD of the primary $[C_{(-H)}Ba]^+$ fragment.

The comparison of the IRMPD spectrum of the $[C_{(-H)}Ba]^+$ complex produced in the ESI with the mass-resolved IRMPD spectrum of $[C_{(-H)}Ba]^+$ formed upon IRMPA of $[C_{(-H)}BaC]^+$ shows that in the ESI source, the $[C_{(-H)}KAN3O-Ba]^+$ isomer is produced in addition to the $[C_{(-H)}KAN1O-Ba]^+$ isomer.

The $[C_{(-H)}KAN1O-Ba]^+$ isomer is the most stable in both the gas and solution phase, while the $[C_{(-H)}KAN3O-Ba]^+$ isomer is the third most stable isomer in the gas phase and it becomes the second most stable structure in solution. The absence of the second most stable $[C_{(-H)}Kl_{anti}^{N1}N3N8-Ba]^+$ isomer in the gas phase suggest that the observed isomers upon ESI are produced in the solution and their structure are maintained upon vaporization.

ACKNOWLEDGMENTS:

This work has been conducted within the International Associated Laboratory LEMIR (CNRS/CONICET) and was supported by CONICET, FONCyT, SeCyT-UNC and by the EU Horizon 2020 Program (CALIPSO Plus and EU_FT-ICR_MS, under grant numbers 730872 and 731077, respectively). GAP thanks the Labex PALM (ANR-10-LABX-0039-PALM) for the invited Professor grant in 2019.

KEYWORDS:

Density functional calculations; DNA-bases; Ions Spectroscopy; Mass spectrometry; Metal cations interactions

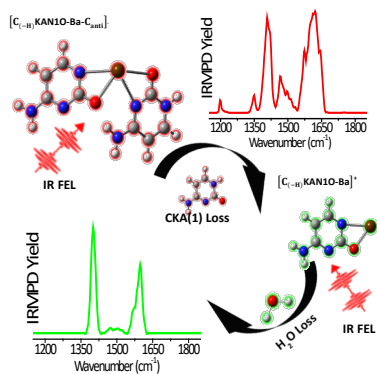
REFERENCES

- [1]. J. D. Watson, F. H. Crick, *Nature*. **1953**, *171*, 737–738.
- [2]. H. Venner, C. Zimmer, *Biopolym*. **1966**, *4*, 321–335.
- [3]. Y. Takezawa, M. Shionoya, *Acc. Chem. Res.* **2012**, *45*, 2066–2076
- [4]. C. Creze, B. Rinaldi, R. Haser, P. Bouvet, P. Gouet, *Acta Crystallogr.* **2007**, *63*, 682–688.
- [5]. B. Debmalya, G.M. Arachchilage, S. Basu, *Front. in Chem.* **2016**, *4*, 38–50.
- [6]. V. Gabelica; F. Rosu, E. De Pauw, J. Lemaire, J-C. Gillet, J-C. Pouilly, F. Lecomte, G. Gregoire, J-P. Schermann, C. Desfrancois, *J. Am. Chem. Soc.* **2008**, *130*, 1810–1811.
- [7]. M. Guéron, J. L. Leroy, *Curr. Opin. Struct. Biol.* **2000**, *10*, 326–331.
- [8]. K. Gehring, J.L. Leroy, M. Gueron, *Nature*. **1993**, *363*, 561–565.
- [9]. B. Yang, M.T. Rodgers, *J. Am. Chem. Soc.* **2013**, *136*, 282–290.
- [10]. G. Féraud, M. Berdakin, C. Dedonder, C. Jouvet, G.A. Pino, *J. Phys. Chem. B.* **2015**, *119*, 2219–2228.
- [11]. K. Hoogsteen, *Acta Crystallogr.* **1963**, *16*, 907–916.
- [12]. A.F. Cruz-Ortiz, M. Rossa, F. Berthias, M. Berdakin, P. Maitre, G.A. Pino, *J. Phys. Chem. Lett.* **2017**, *8*, 5501–5506.
- [13]. S.M. Swasey, L. Espinosa, O. Lopez-Acevedo, J. Pavlovich, E. Gwinn, *Sci. Rep.* **2015**, *5*, 10163–10172.
- [14]. H. A. Day, C. Huguin, Z.A.E. Waller, *Chem. Commun.* **2013**, *49*, 7696–7698.
- [15]. I. Toshihiro, I. Tatsuaki, A. Norie, W.W. Anthony, J. Akinori, *J. Am. Chem. Soc.* **2009**, *131*, 3826–3827.
- [16]. M. Berdakin, V. Steinmetz, P. Maitre, G.A. Pino, *J. Phys. Chem. A.* **2014**, *118*, 3804–3809.
- [17]. J. Gao, G. Berden, M.T. Rodgers, J. Oomens, *Phys. Chem. Phys. Chem.* **2016**, *18*, 7269–7277.
- [18]. J-Y. Salpin, S. Guillaumont, J. Tortajada, L. MacAleese, J. Lemaire, P. Maitre, *Chem. Phys. Chem.* **2007**, *8*, 2235–2244.
- [19]. M. Broquier, S. Soorkia, G.A. Pino, C. Dedonder-Lardeux, C. Jouvet, G. Grégoire, *J. Phys. Chem. A.* **2017**, *121*, 6429–6439.
- [20]. M. Berdakin, G. Féraud, C. Dedonder-Lardeux, C. Jouvet, G.A. Pino, *Phys. Chem. Chem. Phys.* **2014**, *16*, 10643–10650.

- [21]. J. Oomens, A.R. Moehlig, T.H. Morton, *J. Phys. Chem. Lett.* **2010**, *1*, 2891–2897.
- [22]. B. Yang, R.R. Wu, N.C. Polfer, G. Berden, J. Oomens, M.T. Rodgers, *J. Am. Soc. Mass Spectrom.* **2013**, *24*, 1523–1533.
- [23]. M. Berdakin, V. Steinmetz, P. Maitre, G.A. Pino, *Phys. Chem. Chem. Phys.* **2015**, *17*, 25915–25924.
- [24]. E. A. L. Gillis, M. Demireva, K. Nanda, G. Beran, E. R. Williams, T. D. Fridgen, *Phys. Chem. Chem. Phys.* **2012**, *14*, 3304–3315.
- [25]. S. Guillaumont, J. Tortajada, J-Y. Salpin, A.M. Lamsabhi, *Int. J. Mass Spectrom.* **2005**, *243*, 279–293.
- [26]. A.M. Lamsabhi, M. Alcamí, O. Mó, M. Yáñez, J. Tortajada, *J. Phys. Chem. A.* **2006**, *110*, 5, 1943–1950.
- [27]. O.Y. Ali, T.D. Fridgen, *Int. J. Mass Spectrom.* **2011**, *308*, 167–174
- [28]. B. Power, V. Haldys, J-Y. Salpin, T.D. Fridgen, *Int. J. Mass Spectrom.* **2018**, *429*, 56–65.
- [29]. B. Power, V. Haldys, J-Y. Salpin, T.D. Fridgen, *J. Mass Spectrom.* **2016**, *51*, 236–244.
- [30]. B. Power, V. Haldys, J-Y. Salpin, T.D. Fridgen, *Int. J. Mass Spectrom.* **2015**, *378*, 328–335.
- [31]. A. A. Power, O.Y. Ali, M. B. Burt, T.D. Fridgen, *Int. J. Mass Spectrom.* **2012**, *233*, 330–332
- [32]. J-Y. Salpin, V. Haldys, S. Guillaumont, J. Tortajada, M. Hurtado, A.M. Lamsabhi, *Chem. Phys. Chem.* **2014**, *15*, 2959–2971.
- [33]. J.M. Bakker, T. Besson, J. Lemaire, D. Scuderi, P. Maitre, *J. Phys. Chem. A.* **2007**, *111*, 13415–13422.
- [34]. R. Prazeres, F. Glotin, C. Insa, D.A. Jaroszynski, J.M. Ortega, *Eur. Phys. J. D.* **1998**, *3*, 87–93.
- [35]. R.K. Sinha, E. Nicol, V. Steinmetz, P. Maitre, *J. Am. Soc. Mass Spectrom.* **2010**, *21*, 758–772.
- [36]. M.J. Frisch, G.W. Trucks, H.B. Schlegel, G.E. Scuseria, M.A. Robb, J.R. Cheeseman, G. Scalmani, V. Barone, B. Mennucci, G.A. Petersson, H. Nakatsuji, M. Caricato, X. Li, H.P. Hratchian, A.F. Izmaylov, J. Bloino, G. Zheng, J.L. Sonnenberg, M. Hada, M. Ehara, K. Toyota, R. Fukuda, J. Hasegawa, M. Ishida, T. Nakajima, Y. Honda, O. Kitao, H. Nakai, T. Vreven, J.A. Montgomery, J.E. Peralta, F. Ogliaro, M. Bearpark, J.J. Heyd, E. Brothers, K.N. Kudin, V.N. Staroverov, T. Keith, R. Kobayashi, J. Normand, K. Raghavachari, A. Rendell, J.C. Burant, S.S. Iyengar, J. Tomasi, M. Cossi, N. Rega, J.M. Millam, M. Klene, J. E. Knox, J.B. Cross, V. Bakken, C. Adamo, J. Jaramillo, R. Gomperts, R.E. Stratmann, O. Yazyev, A.J. Austin, R. Cammi, C.

Pomelli, J.W. Ochterski, R.L. Martin, K. Morokuma, V. G. Zakrzewski, G.A. Voth, P. Salvador, J.J. Dannenberg, S. Dapprich, A.D. Daniels, O. Farkas, J.B. Foresman, J.V. Ortiz, J. Cioslowski, D. J. Fox, *Gaussian, Inc., Wallingford CT*, **2013**.

- [37]. A.D. Becke, *J. Chem. Phys.* **1993**, *98*, 5648–5652.
- [38] C. Lee, W. Yang, R. Parr, *Phys. Rev. B.* **1988**, *37*, 785–789.
- [39]. I.S. Lim, H. Stoll, P. Schwerdtfeger, *J. Chem. Phys.* **2006**, *124*, 107–113.
- [40]. J.A. Plumley, J.J. Dannenberg, *J. Comput. Chem.* **2011**, *32*, 1519–1527.
- [41]. J.P. Merrick, D. Moran, L. Radom, *J. Phys. Chem. A.* **2007**, *111*, 11683–11700.
- [42]. A.E. Reed, L.A. Curtiss, F. Weinhold, *Chem Rev.* **1988**, *88*, 899–926.
- [43]. W.A. Donald, G.N. Khairallah, R.A.J. O’Hair, *J. Am. Soc. Mass Spectrom.* **2013**, *24*, 811–815.
- [44]. J. Tomasi, B. Mennucci, R. Cammi, *Chem. Rev.* **2005**, *105*, 2999–3093.
- [45]. O.W. Wheeler, D.R. Carl, T.E. Hofstetter, P.B. Armentrout, *J. Phys. Chem. A.* **2015**, *119*, 3800–3815.
- [46]. J. Oomens, D.T. Moore, G. Meijer, G. von Helden, *Phys. Chem. Chem. Phys.* **2004**, *6*, 710–718.
- [47]. A. Simon, W. Jones, J. Ortega, P. Boissel, J. Lemaire, P. Maître, *J. Am. Chem. Soc.* **2004**, *126*, 11666–11674.
- [48]. T.I. Yacovitch, N. Heine, C. Brieger, T. Wende, C. Hock, D.M. Neumark, K.R. Asmis, *J. Phys. Chem. A.* **2013**, *117*, 7081–7090
- [49]. J.P. Beck, J.M. Lisy, *J. Chem. Phys.* **2011**, *135*, 044302/1–044302/6.
- [50]. Y. Zhu, H.A. Roy, N.A. Cunningham, S.F. Strobehn, J. Gao, M.U. Munshi, G. Berden, J. Oomens, M.T. Rodgers, *J. Am. Soc. Mass Spectrom.* **2017**, *28*, 2423–2437.



A sequential IRMPD dynamics is observed in the $[C_{(-H)}BaC]^+$ complex. The $[C_{(-H)}Ba]^+$ is the primary ionic fragment of the $[C_{(-H)}BaC]^+$ complex, while $[C_{(-H)}Ba-H_2O]^+$ is a secondary fragment produced by the subsequent IRMPD of the primary $[C_{(-H)}Ba]^+$ fragment.